Bioinspiration & Biomimetics

PAPER

Design, analysis, and validation of an orderly recruitment valve for bio-inspired fluidic artificial muscles

To cite this article: Dheeraj Vemula *et al* 2022 *Bioinspir. Biomim.* **17** 026001

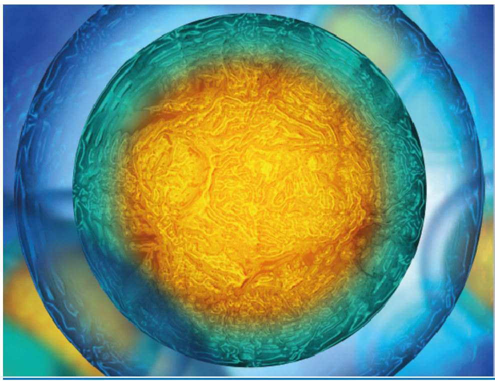

IOP Publishing Bioinspir. Biomim. 17 (2022) 026001 https://doi.org/10.1088/1748-3190/ac4381

Bioinspiration & Biomimetics

RECEIVED
17 August 2021

REVISED
8 December 2021

ACCEPTED FOR PUBLICATION
15 December 2021

PUBLISHED
24 January 2022

PAPER

Design, analysis, and validation of an orderly recruitment valve for bio-inspired fluidic artificial muscles

Dheeraj Vemula, Jeong Yong Kim, Nicholas Mazzoleni and Matthew Bryant*

Intelligent Structures and Systems Research Lab, Department of Mechanical and Aerospace Engineering, North Carolina State University, Raleigh, NC 27695-7910, United States of America

* Author to whom any correspondence should be addressed.

E-mail: mbryant@ncsu.edu

Keywords: fluidic artificial muscle, variable recruitment, McKibben actuator

Abstract

Biological musculature employs variable recruitment of muscle fibers from smaller to larger units as the load increases. This orderly recruitment strategy has certain physiological advantages like minimizing fatigue and providing finer motor control. Recently fluidic artificial muscles (FAM) are gaining popularity as actuators due to their increased efficiency by employing bio-inspired recruitment strategies such as active variable recruitment (AVR). AVR systems use a multi-valve system (MVS) configuration to selectively recruit individual FAMs depending on the load. However, when using an MVS configuration, an increase in the number of motor units in a bundle corresponds to an increase in the number of valves in the system. This introduces greater complexity and weight. The objective of this paper is to propose, analyze, and demonstrate an orderly recruitment valve (ORV) concept that enables orderly recruitment of multiple FAMs in the system using a single valve. A mathematical model of an ORV-controlled FAM bundle is presented and validated by experiments performed on a proof-of-concept ORV experiment. The modeling is extended to explore a case study of a 1-DOF robot arm system consisting of an electrohydraulic pressurization system, ORV, and a FAM-actuated rotating arm plant and its dynamics are simulated to further demonstrate the capabilities of an ORV-controlled closed-loop system. An orderly recruitment strategy was implemented through a model-based feed forward controller. To benchmark the performance of the ORV, a conventional MVS with equivalent dynamics and controller was also implemented. Trajectory tracking simulations on both the systems revealed lower tracking error for the ORV controlled system compared to the MVS controlled system due to the unique cross-flow effects present in the ORV. However, the MVS, due to its independent and multiple valve setup, proved to be more adaptable for performance. For example, modifications to the recruitment thresholds of the MVS demonstrated improvement in tracking error, albeit with a sacrifice in efficiency. In the ORV, tracking performance remained insensitive to any variation in recruitment threshold. The results show that compared to the MVS, the ORV offers a simpler and more compact valving architecture at the expense of moderate losses in control flexibility and performance.

1. Introduction

1.1. FAM background

McKibben artificial muscles or fluidic artificial muscles (FAMs) were first created by their namesake Joseph McKibben as an orthopedic aid for his daughter, who had polio [1]. Inspired by mammalian muscles, FAMs share many similarities with their mammalian counterparts. Just as mammalian muscles are activated by an applied activation energy, FAMs are activated by an applied pressure. Similar to mammalian muscles, FAMs are single-acting contractile actuators with an inverse force-strain behavior [2]. Since FAMs are single-acting, they need an antagonistic pair to act as a double-acting actuator. A typical FAM construction is inexpensive and primarily consists of two concentric elements. The inner component is an elastic bladder embedded within a pantograph structured braided mesh. When pressurized, this bladder expands into the mesh pushing it radially outwards. The outer mesh, due to its pantograph structure, expands radially while contracting axially, thus producing a contractile force. The force-strain behavior of a FAM is governed by the applied pressure and the elements of its construction geometry such as the initial radius, length and braid angle. Therefore, a wide range of force-strain profiles can be obtained by altering the applied pressure or the construction of the FAM.

FAMs are popular and widely studied due to their inherent compliance, low cost, large displacements, high force-to-weight ratio, and similarity to mammalian muscles in actuation [3, 4]. Tiwari *et al* compared an antagonistic pair of FAMs to an equivalent double-acting cylinder and found that FAMs were able to achieve a force-to-weight ratio that is six times greater at 1/10th the price of a cylinder [5]. These advantages present artificial muscles as an attractive option for actuation in humanoid robots [6], prosthetics and rehabilitation robots [7–10]. Until recently, researchers have only studied pneumatic FAMs. However, since these systems use compressed air as operating fluid, pneumatic FAMs present certain limitations on performance characteristics such as response time when compared to traditional piston cylinder actuators [11]. In addition, due to characteristics inherent to pneumatic systems such as high compressibility and leakage, these systems tend to have lower efficiency.

Most researchers have studied pneumatic FAMs, but more recently hydraulic FAMs have been proposed [5]. While pneumatic actuation simplifies the fluid circuit, avoids messy hydraulic fluids, and offers high compliance, it also presents limits on performance characteristics such as response time and efficiency [4]. Meller *et al* compared hydraulic and pneumatic actuation of FAMs and found that hydraulic FAMs have advantages in efficiency [12]. Hydraulic FAMs have been found to be 180% more energy efficient in producing the same amount of mechanical energy while considering the energy required to compress the working fluid. This trait in hydraulic FAMs has been attributed to lower compressibility of hydraulic fluid when compared to pneumatic fluid such as air.

1.2. Variable recruitment in FAMs

In mammalian muscles, individual muscle fibers are bundled together to form larger motor units [13]. The individual muscle fibers within the larger bundles are recruited based on Henneman's size principle, which states that muscle fibers are recruited in an orderly fashion from smaller units to larger units as load requirement increases [14]. As the smaller units are less prone to fatigue, this strategy minimizes fatigue in the muscle for low load conditions while enabling fine motor control at all operating conditions. Employing a similar principle in FAM bundles, researchers have shown a two-fold improvement in average efficiency with a variable recruitment muscle bundle when compared to a single equivalent motor unit, also called a SEMU [15]. This strategy uses the least number of individual muscles or motor units within the bundle that are required based on the applied load and enables most of the motor units to be near ideal operating pressure while minimizing the fluid volume consumption and throttling losses. This variable recruitment principle has been implemented primarily through two different methodologies, passive variable recruitment (PVR) and active variable recruitment (AVR), both of which are discussed in the following sections.

1.3. Active variable recruitment

An AVR system provides the flexibility to control each motor unit in the system independently. Until now AVR was implemented through a 'multi-valve system' (MVS) configuration where each motor unit in the system is controlled through a discrete valve. Meller *et al* implemented an online AVR strategy with a MVS to control a FAM bundle with three pairs of muscles [16]. The researchers incorporated three recruitment levels in the muscle bundle. Progression from lower recruitment level to higher recruitment level would happen when the current muscle reaches a prescribed recruitment pressure. The recruitment pressure can be tailored to the required load and thus can be operated at maximum efficiency for a wide range of loads. However, with a multi-valve configuration, the system requires as many valves as the number of motor units within the system. This increases complexity and weight of the entire system which can be detrimental in applications such as mobile robotics or wearable exoskeletons where artificial muscle systems are being widely used.

1.4. Passive variable recruitment

A system with PVR uses differences in the mechanical design and/or material properties of the individual motor units within a muscle bundle to achieve variable recruitment [17]. Akin to threshold energy that is required for activation of the muscle fiber in mammalian muscles, FAMs require a minimum pressure called threshold pressure to start generating contraction. This threshold pressure for a FAM is derived based on the geometry and material properties of the FAM. A FAM system with PVR consists of a single control valve that controls the pressure to the entire bundle and multiple motor units with distinct threshold pressures. When a certain pressure is applied, all the muscles whose threshold pressure is less than the applied pressure are activated. Chapman & Bryant showed that a PVR bundle is more efficient compared to a single equivalent motor unit in low load conditions [17]. This strategy can be advantageous since it uses a single control valve for the entire bundle. However, higher threshold pressure in the FAM design means that greater elastic energy is stored in the actuator, reducing the actual work output of the system. Thus, a PVR system offers efficiency advantages only in a certain range of operating conditions and is therefore less versatile than an AVR system.

1.5. Current study

The research presented in this paper focuses on the design and analysis of an orderly recruitment valve (ORV) that aims to strike a balance between the performance and flexibility of the AVR–MVS and the single valve simplicity of the PVR architecture. Compared to an MVS, which would require n number of valves corresponding to n number of FAMs. The proposed ORV only requires one valve to control the pressures of multiple FAMs, reducing the bulkiness of the overall system. As discussed in section 2, the increased number of output ports would result in a larger valve body, but the advantage of a decrease in the number of valves would outweigh such effects. In section 2, an analytical model of an ORV-controlled FAM bundle is presented and validated experimentally. In section 3, a case study of a one degree of freedom (1-DOF) robotic arm with hydraulic FAM actuators using the ORV is presented. A model-based feedforward control system is developed to control the valve system to track a prescribed trajectory. The results and discussions of the trajectory tracking simulations for the ORV and a comparative study of the ORV with an equivalent multivalve system from the case study are presented. Performance characteristics such as efficiency and integrated absolute error (IAE) are evaluated across a range of trajectories. Lastly, conclusions summarizing the modeling and trajectory tracking simulations are presented in section 4 along with the scope for future work.

2. Modeling and validation of the ORV-controlled FAM bundle

2.1. Valve modeling

2.1.1. Design of the ORV

The design goal of the ORV is to enable activation of multiple FAM motor units in a sequential manner just as we see in mammalian muscles. For the purpose of demonstration, a simple design for the ORV that can work with two motor units is proposed and considered throughout this paper. In practice, a single ORV is capable of activating more than two motor units as illustrated in figure 1. The ORV assembly primarily consists of two components, a valve body and a linear sliding spool. The valve body consists of a supply port, a reservoir port and two ports for the FAM motor units. The FAM ports are normally venting to the reservoir and as the spool travels from the left of the valve body to the right, it opens the FAM ports to the supply port while sequentially pressurizing them. In a similar manner, by moving the spool in the other direction, the valve can sequentially vent each muscle to the reservoir. This arrangement mechanically encodes the orderly recruitment/de-recruitment sequence in a single valve. However, this mechanical encoding sacrifices the ability to exclude motor units from the recruitment sequence if desired, which could be advantageous in cases of damage to a subset of motor units. If such functionality is needed in an ORV-based system, small on/off type valves could be added at each outlet port of the ORV to isolate failed FAMs. However, this would increase mechanical complexity.

The simplicity of the proposed design facilitates an easy extension for any number of motor units depending on the system requirement. This could be accomplished by making the valve housing larger, extending the spool travel, and then increasing the number of outlet ports between the supply port and reservoir port. This layout of the ORV introduces a unique geometric element in its dead band, x_{db}. The dead band is defined as the clearance between two consecutive FAM input ports.

The ORV geometry as shown in figure 2 is assumed to be critically lapped which means that the spool width, x_{sw} is equal to the port opening diameters, $x_{v,1}$, $x_{v,2}$ and $x_{v,n}$, where n is the number of ports [18]. As the number of ports increase, the rod length, x_{r} that connects the two spools increases as well. The proposed ORV design uses a linear sliding spool but, in effect, the same sequential activation can be achieved using a rotary-type spool, for which the diameter of the spool would increase as the number of output ports increase. The dead band, x_{db} is sized to avoid any overlap between ports during operation thus making it equal to the spool width. By transitive relation this makes the dead band equal to port diameters as shown in equation (1).

$$x_{v,1} = x_{v,2} = x_{\mathrm{sw}} = x_{\mathrm{db}}. \tag{1}$$

In order to effectively characterize the performance of the ORV, an analytical model is developed that emulates the pressure flow dynamics and the spool dynamics.

2.1.2. Flow dynamics

Due to its design, the ORV exposes multiple FAM ports to each other during actuation when the spool is at extreme positions as shown in figures 1(a) and (c). In addition to traditional flow between the supply and input ports or input and reservoir ports, the ORV introduces flow coupling between multiple FAM input ports termed as 'flow' This cross-flow across FAMs occurs whenever there is a pressure differential, which happens during the transient phase of variable recruitment. This is evident in the flow equations for the valve which is modeled based on orifice flow. As described in equation (4), the cross-flow term Q_{cf} is a function of the individual FAM pressures P_1 and P_2 accumulator pressure P_{s}, flow coefficient c_v and the

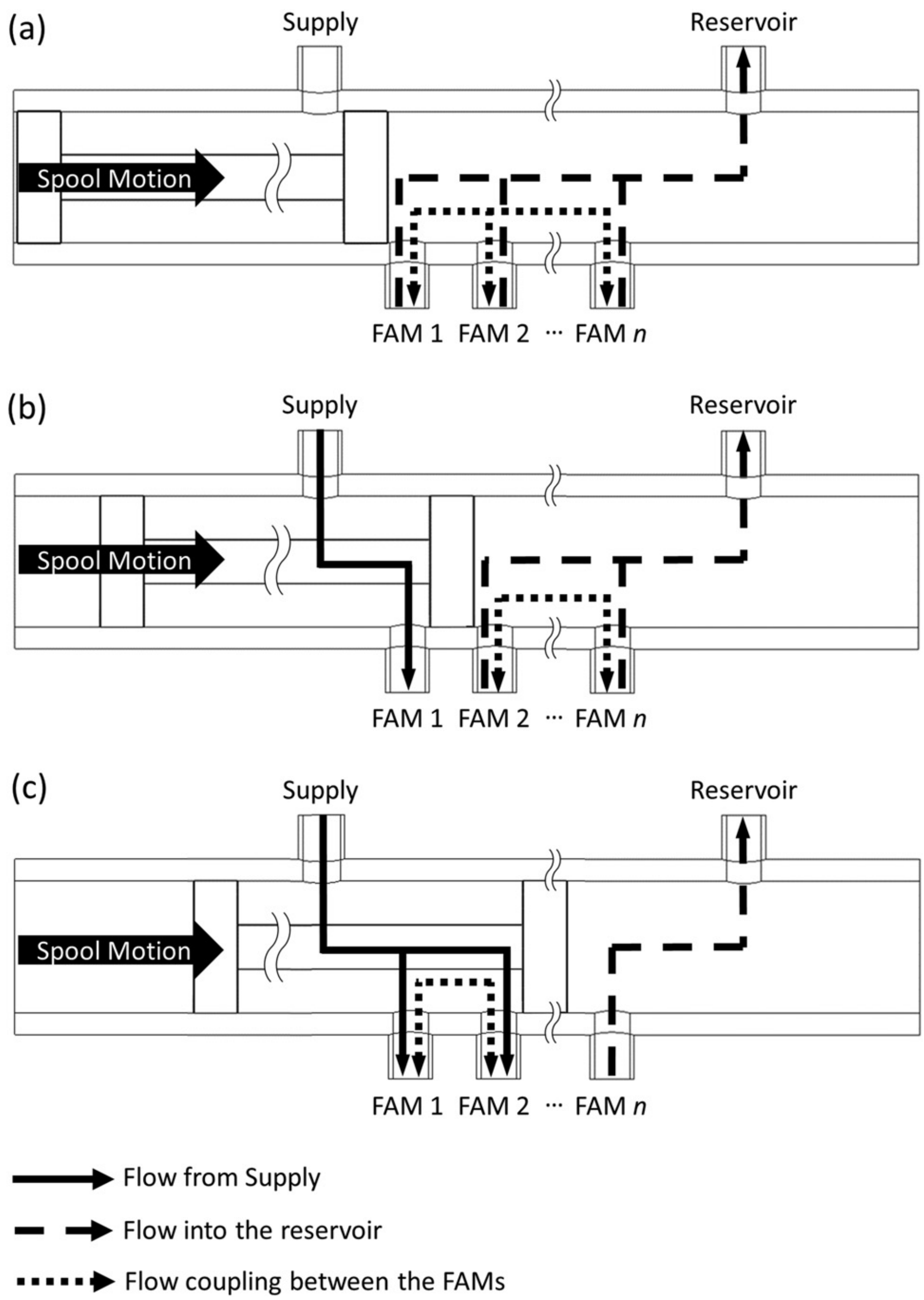

Figure 1. Schematic showing different phases of the ORV.

port openings $x_{v,1}$ and $x_{v,2}$.

$$Q_1 = c_v x_{v,1} \ \mathrm{sgn}\left(P_s - P_1\right) \sqrt{|P_s - P_1|} - Q_{cf}, \quad (2)$$

$$Q_2 = c_v x_{v,2} \ \mathrm{sgn}\left(P_s - P_2\right) \sqrt{|P_s - P_2|} + Q_{cf}, \quad (3)$$

$$Q_{cf} = c_v \ \max\left(x_{v,1}, x_{v,2}\right) \mathrm{sgn}\left(P_1 - P_2\right) \sqrt{|P_1 - P_2|}. \quad (4)$$

The flow coefficient, c_v is calculated as shown in equation (5) based on the nominal flow data of the valve.

$$c_v = \frac{Q_N}{\sqrt{\Delta p_N/2}} \frac{1}{x_{v,\max}}, \quad (5)$$

where Q_N is the nominal flow, Δp_N is the nominal pressure drop, and $x_{v,\max}$ is the maximum stroke of the valve.

2.1.3. Valve spool dynamics

The spool travel in the ORV determines different recruitment levels for the FAM bundle, therefore the spool dynamics are vital in understanding the dynamics of the ORV. A second order system is used to model the spool dynamics for the ORV [19]. The spool position, x_v, is dependent on the valve parameters such as natural frequency, ω_v, gain, K_v, damping coefficient, D_v, hysteresis, f_{hs}, and the input signal, u_v.

$$\frac{1}{\omega_v^2}\ddot{x}_v + \frac{2D_v}{\omega_v}\dot{x}_v + x_v + f_{hs} \ \mathrm{sgn}\left(\dot{x}_v\right) = K_v u_v. \quad (6)$$

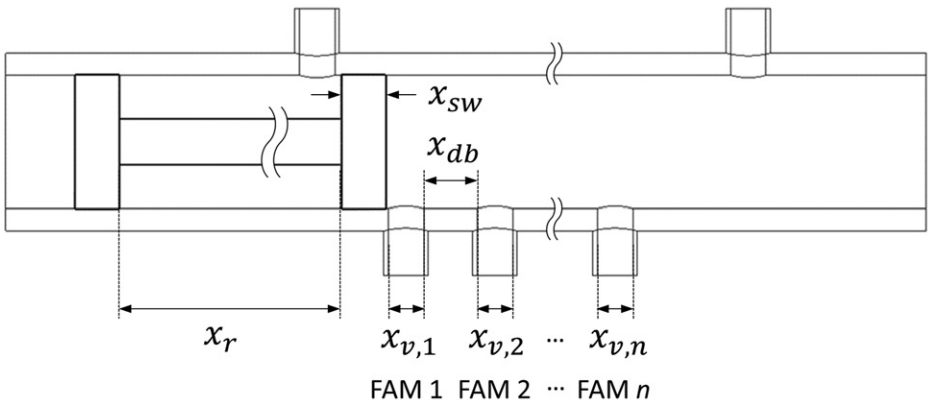

Figure 2. ORV geometry.

A full stroke motion in a traditional valve ranges from the opening to closing of one port, however the ORV has two ports as it controls two FAM motor units. Therefore the full stroke of the ORV should range from the opening of the first port to the closing of the second port which also includes the dead band region in between the two ports. Since the dimensions of the ports are assumed to be identical and are equal to that of the dead band, the total stroke for the ORV is thrice that of a traditional valve.

2.2. FAM modeling

2.2.1. FAM force characterization

For this research, an ideal FAM model is considered which approximates the shape of the muscle to a perfect cylinder and also assumes the intrinsic mechanical properties of the braided outer mesh and the inner elastic tube to be negligible. Tondu & Lopez developed a geometric model for ideal muscles that establishes a relation between the FAM contraction x_{m} the FAM volume V_{m} and the initial FAM geometry such as the length, l_0, radius r_0, and braid angle α_0, as shown in equations (7) and (8) [20].

$$V_{\mathrm{m}} = \pi r_0^2 l_0 \left[b\left(1 - \frac{x_{\mathrm{m}}}{l_0}\right) - \frac{a}{3}\left(1 - \frac{x_{\mathrm{m}}}{l_0}\right)^3 \right], \quad (7)$$

$$a = \frac{3}{\tan^2 \alpha_0}, \qquad b = \frac{1}{\sin^2 \alpha_0}. \quad (8)$$

An ideal FAM model is developed based on the virtual work principle that relates the fluid energy to the mechanical work done as shown in equation (9)

$$P\delta V_{\mathrm{m}} = F\delta x_{\mathrm{m}}, \quad (9)$$

where F_{m} is the axial force output of the FAM, δx_{m} is the FAM contraction along the line of action of the force, P is the FAM pressure and δV_{m} is change in the FAM volume. Differentiating the muscle volume V_{m} with respect to the FAM contraction x_{m} and rearranging equation (9) for force yields the relation between muscle force, pressure, geometry and contraction as shown in equation (10).

$$F_{\mathrm{m}} = \pi r_0^2 P \left[a\left(1 - \frac{x_{\mathrm{m}}}{l_0}\right)^2 - b \right]. \quad (10)$$

2.2.2. FAM pressure dynamics

The transient phase of variable recruitment is important to precisely evaluate the dynamics of the system. The pressure dynamics of the FAM influence its force and consequently the overall plant dynamics. The pressure growth in the FAM is due to the compression of fluid volume in the muscle. Assuming isothermal compression of the fluid, as the volume rate of fluid into the muscle is greater than the volume rate of change of the muscle, pressure within the muscle grows as shown in equation (11)

$$\frac{\mathrm{d}P}{\mathrm{d}t} = \frac{1}{\beta}\frac{Q - \dot{V}_{\mathrm{m}}}{V_{\mathrm{m}}}, \quad (11)$$

$$\dot{V}_{\mathrm{m}} = \pi r_0^2 \left[a\left(1 - \frac{x_{\mathrm{m}}}{l_0}\right)^2 - b \right] \dot{x}_{\mathrm{m}}, \quad (12)$$

where β is the compressibility of fluid and $\dot{V}_{\mathrm{m}}$ is the rate of change of the FAM volume. $\dot{V}_{\mathrm{m}}$ is a function of the FAM contraction velocity $\dot{x}_{\mathrm{m}}$ and is obtained by differentiating FAM volume (equation (7)) with respect to time as shown in equation (12). Since the range of operating pressures in the FAM is small enough $(0 - 750$ kPa), β is assumed to be constant throughout the pressure growth cycle of the FAM.

2.3. Validation experiment

A simple proof-of-concept ORV was built to demonstrate its ability to activate multiple FAMs in sequence as well as its cross-flow effect due to the flow dynamics of the valve design. Although the demonstration can easily be extended to more FAMs, an ORV capable of activating two motor units (for the sake of simplicity) was built and tested and its pressure and contraction measurements compared to simulations using the modeling described in the previous subsections.

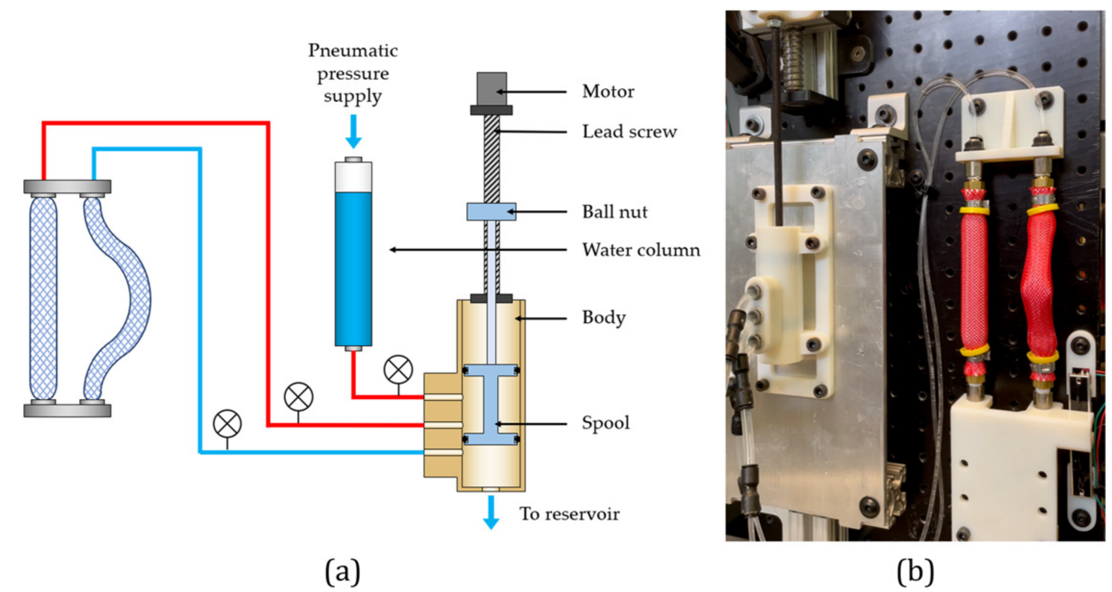

Figure 3. ORV proof-of-concept experiment: (a) hydraulic circuit setup with water column and (b) picture of actual setup.

The ORV body and spool were manufactured using a PolyJet 3D printer (Stratasys Objet30). The body consisted of four ports each corresponding to connections to the supply, FAM 1, FAM 2, and reservoir. This allows for the orderly recruitment of a variable recruitment bundle with two recruitment states, with each FAM acting as the motor unit for its corresponding recruitment state. The bundle is said to be in recruitment state 1, when only the first FAM is activated. When the first FAM reaches the source pressure and the second FAM is activated, the bundle is said to be in recruitment state 2. The spool consisted of two pistons that separate the high-pressure chamber from the environment. Each piston was designed with two grooves, for which O-rings were assembled to ensure seals even when the pistons travel past ports. A valve body inner diameter of 0.0254 m was used with port diameters of 0.003 m. For this simulation, the flow coefficient for the proof-of-concept valve was determined using a generic equation used for a valve, for which the nominal flow and nominal pressure drop are unknown.

$$c_v = \pi d_v \alpha_\mathrm{d} \sqrt{\frac{2}{\rho}}, \tag{13}$$

where d_v is the spool diameter, α_d is the discharge coefficient, and ρ is the fluid density. A theoretical value of $\alpha_\mathrm{d} = 0.611$ is used for the discharge coefficient. The spool was connected to a rod that was actuated linearly using a ball screw driven by a stepper motor. A constant spool travel speed of 9.25×10^{-4} m s^{-1} was used. To fully demonstrate the effect of crossflow between FAMs, experiments were conducted hydraulically, implemented via a pneumatically-pressurized water column as was formerly used by Meller *et al* [16]. The water column was connected to a pneumatic pressure source, for which the pressure was controlled using a regulator and set to 207 kPa(30 psi). The pressures of the water column, FAM 1, and FAM 2 were measured using pressure transducers (TE Connectivity MSP300), all physically located near the ORV to best eliminate pressure changes within the conduit. The valve was connected to a two-motor unit FAM bundle and the contraction of the bundle was measured using a linear potentiometer. Both FAMs were of length 0.127 m, inner radius 0.0064 m, and an initial braid angle of 29.67°. A constant load of 11.1 N(2.5 lbf) was applied by hanging a weight from the bundle. While the construction and spool actuation mechanism of this proof-of-concept experiment is much simpler than a fully-integrated electrohydraulic orderly recruitment servo valve, which would use a hydraulic pilot stage or linear motor to actuate the spool position like any other servo valve [18, 19], it exhibits the essential ORV functionality and pressure dynamics features for model validation (figure 3).

In this demonstration of ORV functionality, the spool was actuated at a constant velocity. The spool was initially positioned such that the high-pressure supply source was not directed to any of the FAM ports. As the spool travels, the ports connected to FAM 1 and FAM 2 are sequentially opened, directing the high-pressure fluid into the actuators. The pressure and contraction measurements from the experiment are shown in figure 4.

Figure 4 shows the sequential activation of FAM 1 and 2, for which the pressures were initially close to zero. As the first port was opened and fluid was allowed to flow to FAM 1, the pressure increased thus activating FAM 1. A momentary drop in the source pressure was observed due to decompression of fluid as it filled the increasing internal volume of FAM 1 during contraction. Eventually, the pressure of FAM

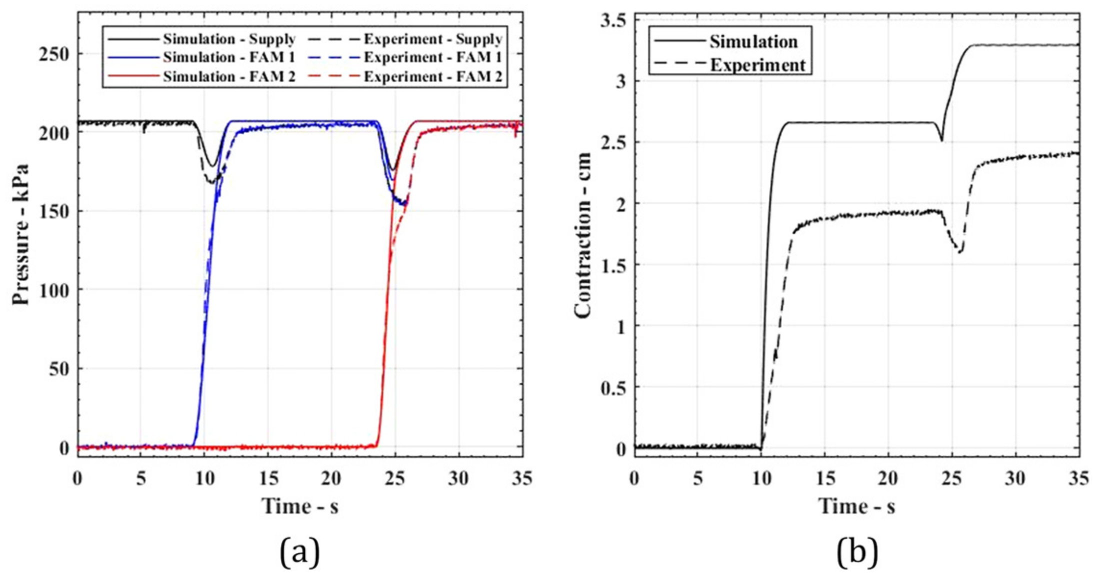

Figure 4. Pressure and contraction of supply, FAM 1 and FAM 2 from experiment and simulation. Both experiment and simulation show sequential activation of two FAMs using a single ORV while showing cross-flow behavior. Discrepancies in the contraction data can be attributed to the ideal FAM model's tendency to overpredict strain.

1 converged to that of the supply, which returned to its initial value. Notably, the cross-flow effect that is unique to the ORV was observed during the activation of the second FAM. The flow coupling of FAM 1 and 2 that has been modeled in equations (2)–(4) was seen as drops in pressures for both the supply and FAM 1 as the pressure of FAM 2 increased. After the spool had traveled to its final position at which both FAM ports were fully open to the supply, both FAM pressures converged to that of the supply. Figure 4 also shows the model simulation results using identical conditions. Due to the use of a water column, the working fluid in the system was modeled as a mixture of air and water with an empirically identified bulk modulus of 9.89×10^4 kPa at the supply pressure of 207 kPa(30 psi). This bulk modulus value was assumed to be constant throughout the simulation.

Overall, the simulation shows good agreement with the experimental measurements. First of all, the valve's functionality of sequentially activating multiple FAMs was evident both in the experiment and simulation. Additionally, the simulation was able to accurately capture the pressure drop of FAM 1 during the activation of FAM 2, which can be credited to the cross-flow effect as modeled in equations (2)–(4). However, discrepancies between the experiment and simulation do exist which can be mostly attributed to the FAM model used. Although the ideal FAM model used in the study is widely used in literature due to its simplicity, it overpredicts strain values and does not take into account pressure-dependent free strain behavior Although recent models have built upon the ideal model using advanced modeling methods and empirical tuning to account for such behavior [1, 15, 21–25], the FAM model used in this study is appropriate for the purpose of demonstrating the functionality of the ORV, as qualitative trends show a good match between the experiment and simulation as seen from figure 4.

3. Case study: actuation and control of a 1-DOF robot arm

3.1. System modeling

In addition to the valve and FAM modeling presented in the previous section, other components necessary to develop and simulate a single degree of freedom rotating arm consisting of the following subsystems, as illustrated in figure 5, are presented in this section:

(a) ORV
(b) Actuation system with two FAM motor units
(c) A rotating arm assembly with a pulley, arm and an end mass
(d) Hydraulic power unit with a motor-pump assembly and an accumulator

Analytical models for each of these subsystems are developed to simulate the overall system dynamics. These models are then used to simulate and compare the performance of the ORV with a conventional multi-valve setup that is required for AVR.

3.1.1. Rotating arm plant modeling

A rotating arm plant is chosen to simulate varying loads on the muscle bundle to trigger recruitment of different FAM motor units. As illustrated in figure 5, the plant consists of a rotating robotic arm-pulley assembly with a mass at the tip. The pulley of mass m_p and radius r_p is connected to a FAM bundle consisting of two parallel FAM motor units. The contractile force F_{bundle} of the FAM bundle translates into a torque

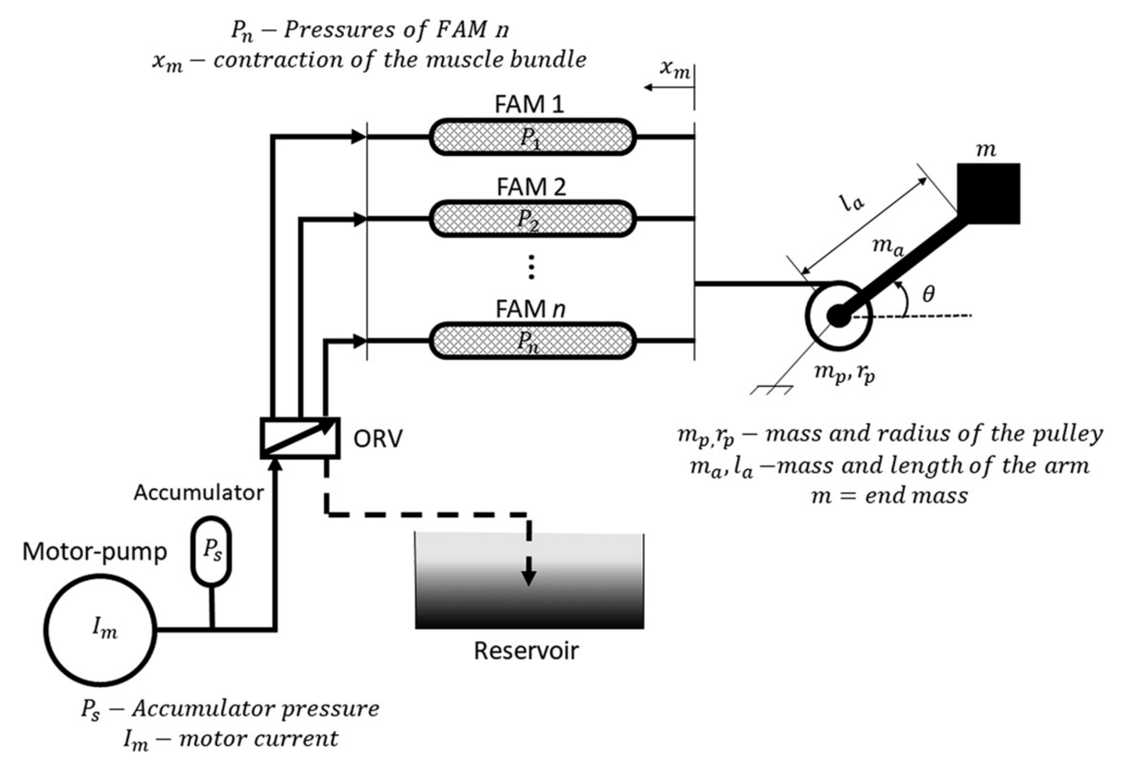

Figure 5. Schematic with different subsystems in the model.

on the pulley, which is counteracted by an external torque τ_{load} due to the mass of the robotic arm m_a and the tip mass m. The equations of motion of the system relating the FAM forces and the angular displacement of the arm θ are given in equations (14) and (15) where I is the moment of inertia of the system and c is the damping within the system.

$$\tau_{\text{net}} = F_{\text{bundle}} r_{\text{p}} - \tau_{\text{load}} = I\ddot{\theta} + c\dot{\theta}, \tag{14}$$

$$\tau_{\text{load}} = mgl_{\text{a}} \cos\theta + m_{\text{a}} g \frac{l_{\text{a}}}{2} \cos\theta. \tag{15}$$

The bundle contraction $x_{\text{m,bundle}}$ and arm angle are related as shown in equation (16):

$$x_{m,\text{bundle}} = l_0 - r_{\text{p}}\theta. \tag{16}$$

3.1.2. Hydraulic power unit modeling

The hydraulic subsystem comprises of a pressure source and hydraulic fluid. The pressure source consists of a motor-pump assembly connected to an accumulator that governs the inlet pressure for the valve system. Modeling the dynamics of the motor pump assembly and the accumulator is essential to simulate the dynamics of supply pressure to the FAMs. Due to the volume consumed by the FAMs during contraction, there is a drop in the pressure of the accumulator, P_{s} which is modeled using ideal gas law while assuming that the temperature is constant as shown in equation (17):

$$P_{\text{s}} = \frac{P_{\text{si}} V_{\text{si}}}{V_{\text{si}} + \left(V_{\text{m},1} + V_{\text{m},2}\right) - V_{\text{p}}}, \tag{17}$$

where P_{si} and V_{si} are the initial pressure and volume of the gas charged accumulator, $V_{\text{m},1}$ and $V_{\text{m},2}$ are the volumes consumed by the FAMs and V_{p} is the volume of fluid pumped by the motor.

The motor-pump assembly, which is assumed to use a positive displacement pump is under constant operation to maintain the accumulator pressure above the set pressure, hence it is important to model the motor-pump dynamics. The motor-pump dynamics are derived from first principles and Kirchhoff's voltage law as given in equations (18) and (19).

$$\ddot{\theta}_{\text{p}} = \frac{K_{\text{m}} I_{\text{m}} - \tau_{\text{p}}}{J_{\text{p}}}, \tag{18}$$

$$\dot{I}_{\text{m}} = \frac{V_{\text{motor}} - k_{\text{b}}\dot{\theta}_{\text{p}} - I_{\text{m}} R_{\text{m}}}{L_{\text{m}}}. \tag{19}$$

The motor parameters such as current, coil inductance, coil resistance, back emf constant, torque constant and supply voltage are given by I_{m}, L_{m}, R_{m}, k_{b}, K_{m}, and V_{motor} respectively and the pump parameters such as the angular displacement, rotational inertia and impeller torque are given by θ_{p}, J_{p}, and τ_{p}, respectively.

3.2. Control approach

3.2.1. Orderly recruitment switching logic

Orderly recruitment is a bio-inspired variable recruitment strategy that sequentially recruits FAM units based on the applied load. In biological musculature new motor units are recruited in a sequential manner from smaller to larger units as the load increases. Employing a similar strategy, a switching logic is used to recruit FAM units in an orderly manner based on the applied load.

The switching logic determines the recruitment state, RS, based on the required pressure from the FAM bundle and the supply pressure as shown in equation (20) for a FAM bundle of two units.

$$\mathrm{RS} = \begin{Bmatrix} 1, P_{\mathrm{req}} < P_{\mathrm{s}} \\ 2, P_{\mathrm{req}} \geqslant P_{s} \end{Bmatrix}. \tag{20}$$

Here RS = 1 represents recruitment on the first FAM motor unit and RS = 2 represents recruitment of both FAM motor units. Pressure required is estimated based on the required force, F_{req} from the FAM and required FAM contraction $x_{\mathrm{m,req}}$, as shown in equation (21).

$$P_{\mathrm{req}} = \frac{F_{\mathrm{req}}}{\pi r_0^2\left[a\left(1-\frac{x_{m,\mathrm{req}}}{l_0}\right)^2 - b\right]}. \tag{21}$$

F_{req} and $x_{\mathrm{m,req}}$ are estimated based on the load applied (equations (14), (15) and (17)) and the reference position, θ_{ref} as shown in equations (22) and (23).

$$F_{\mathrm{req}} = \frac{I\ddot{\theta}_{\mathrm{ref}} + c\dot{\theta}_{\mathrm{ref}} + mgl_{\mathrm{a}}\cos\theta_{\mathrm{ref}} + m_{\mathrm{a}}g(l_{\mathrm{a}}/2)\cos\theta_{\mathrm{ref}}}{r_{\mathrm{p}}}, \tag{22}$$

$$x_{\mathrm{m,req}} = l_0 - \theta_{\mathrm{ref}} r_{\mathrm{p}}. \tag{23}$$

3.2.2. Controller implementation

There is an abundance of literature on controller development for pneumatic artificial muscles [26], with more recent developments in control systems for hydraulic artificial muscles [27].

Meller *et al* developed a model-based feed forward PI controller for hydraulic artificial muscle system with variable recruitment that can improve performance tracking due to its ability to take predictive action [28]. However, this implementation uses linearization to identify the flow gain of the controller for a commanded input signal to the valve. Due to the transient phase in the orderly recruitment used in the current research, the linearization approximation does not consider the pressure dynamics. Inspired from the linearized feed forward controller and the gap in its approximations, an updated controller is developed to suit the orderly recruitment strategy.

3.2.2.1. Feed forward controller with orderly recruitment. The objective of the updated controller is to address the linearization approximations through an inverse dynamics model that is used to estimate the relation between spool position and reference trajectory. The feed forward model needs two stages of parameter estimation to accurately provide a feed forward input. The first stage is the required pressure estimation from equation (21) and second stage is the required valve input estimation. After estimating the required pressure as shown in equation (21), the next step is to estimate the required spool position, $x_{v,\mathrm{req}}$ based on the estimated pressure and required flow rate, $Q_{\mathrm{m,req}}$ as shown in equation (24):

$$x_{v,\mathrm{req}} = \frac{Q_{\mathrm{m,req}}}{c_v\sqrt{\left|P_{\mathrm{s}}(t) - P_{\mathrm{req}}\right| \mathrm{sgn}(P_{\mathrm{s,req}} - P_{\mathrm{req}})}}, \tag{24}$$

where $Q_{\mathrm{m,req}}$ is the required flow rate from the valve and $P_{\mathrm{s}}(t)$ is the supply pressure. $Q_{\mathrm{m,req}}$ is estimated based on the required FAM contraction as shown in equation (25) and $P_{\mathrm{s}}(t)$ is a function of hydraulic subsystem's initial states and the reference trajectory.

$$Q_{\mathrm{m,req}} = \pi r_0^2\left[a\left(1-\frac{x_{\mathrm{m,req}}}{l_0}\right)^2 - b\right]\dot{x}_{\mathrm{m,req}}. \tag{25}$$

After estimation of the required spool position, the corresponding valve feed forward input, u_{ff} is calculated based on inverting the spool dynamics from equation (6) as shown in equation (26).

$$u_{\mathrm{ff}} = \frac{\left[\frac{1}{\omega_v^2}\ddot{x}_{v,\mathrm{req}} + \frac{2D_v}{\omega_v}\dot{x}_{v,\mathrm{req}} + x_{v,\mathrm{req}} + f_{\mathrm{hs}}\ \mathrm{sign}(\dot{x}_{v,\mathrm{req}})\right]}{K_v}. \tag{26}$$

The feed forward estimation for a single FAM shown above is extended for a FAM bundle based on the recruitment state, RS. A PI feedback loop is added to this feed forward controller whose overall control law is shown in equation (27):

$$u_v = u_{\mathrm{ff}} + u_{\mathrm{pi}}, \tag{27}$$

where the PI control input, u_{pi} is a function of the PI gains and the trajectory error e, as shown in equations (28) and (29) respectively.

$$u_{\mathrm{pi}} = K_{\mathrm{p}}e + K_{\mathrm{i}}e, \tag{28}$$

$$e = \theta_{\mathrm{ref}} - \theta. \tag{29}$$

As shown in figure 6, the overall control architecture of the system consists of six primary blocks. The control structure developed in this section is used to control the system model developed in the previous section to track a prescribed trajectory. These trajectory tracking simulations were used to characterize the behavior of the ORV.

3.3. Subsystem and simulation parameters

The parameters used in all simulation subsystems are listed in table 1.

The valve is sized and modeled based on a commercial servovalve, MOOG G761, and all the required parameters for the valve model are obtained from the manufacturer's catalog of the MOOG valve. The parameters of the arm were chosen to approximate a lab-scale robot arm apparatus, and the FAM parameters were set to that of previous experiments (e.g. Meller *et al* [16]) that are reasonable for the scale of the arm. The motor-pump parameters were taken from the actual parameters of a motor used

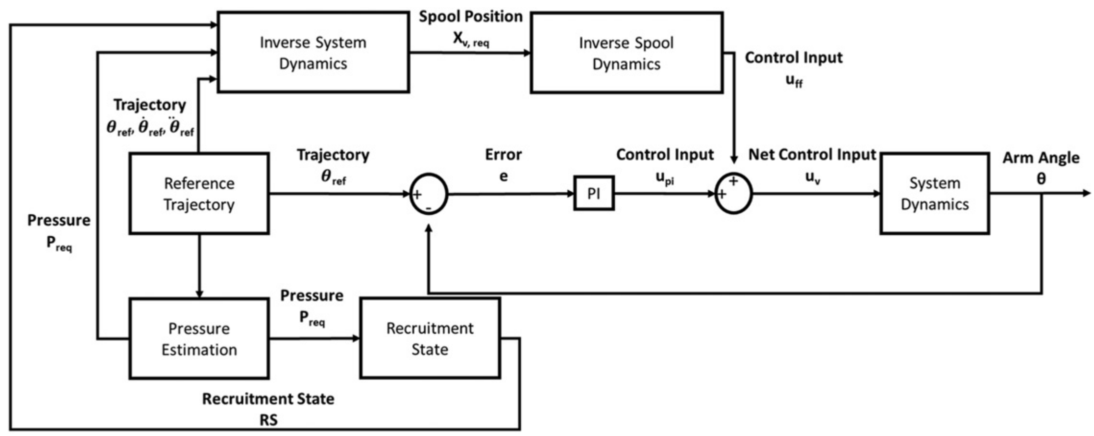

Figure 6. Block diagram showing the control structure of the feed forward PI controller along with different signal flows in the system.

Table 1. Parameters used for different subsystems.

Muscle		Accumulator	
Parameter	Value	Parameter	Value
r_0 (cm)	0.64	P_{si} (kPa)	760
l_0 (cm)	17.78	V_{si} (m^3)	0.00038
α_0 (deg)	29.67		
Motor-pump		**Rotary arm**	
Parameter	Value	Parameter	Value
L_m (H)	0.00011	m_p (kg)	1
R_m (ohms)	0.45	r_p (m)	0.05
k_b (rad V^{-1} s^{-1})	0.017	m_a (kg)	0.5
K_m (Nm A^{-1})	0.017	l_a (m)	1
V_m (V)	10	m (kg)	2.2
J (kg m^2)	9.45×10^{-5}	c (Ns m^{-1})	0.029
Valve flow		**Spool dynamics**	
Parameter	Value	Parameter	Value
K_v	10	Δp_n (kPa)	350
D_v	1	Q_n (l m^{-1})	63
ω_v (Hz)	1800	$x_{v,\max}$ (mm)	10.82
f_{hys} (%)	3		
Hydraulic fluid			
Parameter			Value
$1/\beta$ (kPa)			2.15×10^6

for a mobile robotics application [17]. The accumulator pressure is characteristic of the pressures at which FAMs are operated, and accumulator volume was chosen to be 10 times the volume of the FAMs themselves. The bulk modulus parameter of the hydraulic fluid, 2.15×10^6 kPa, falls within the acceptable range of 1.88×10^6 kPa to 2.49×10^6 kPa [29], and is consistent with other online manufacturer data tables. The gains for the PI controller ($K_p = 53.1$ V rad^{-1}, $K_i = 27.2$ V rad^{-1}) were tuned based on Ziegler–Nichols method with further refinement through hand tuning.

3.4. Case study results and discussion

To illustrate the dynamics of the system and demonstrate characteristics of the ORV, a series of trajectory tracking simulations for the rotating arm angle are developed. Half-sine trajectories with varying arm angles and tip masses are used to simulate a parametric case study. The feed forward PI controller developed in section 3.2.1 is used to track the reference trajectories. Since the objective of this study was to characterize the ORV, the controller was assumed to be ideal with zero modeling errors.

3.4.1. Recruitment phase

A half-sine trajectory with a frequency of 1 Hz (which translates into a time span, $\Delta t = 0.5$ s) and arm angle travel from -20 degrees to 0 degrees is simulated. FAM 1 was initialized with a pressure just enough to start the simulation from an equilibrium. A tip mass ($m = 2.2$ kg) is chosen so that the first FAM reaches saturation at an arm angle of -13 degrees, at which the second muscle recruitment begins. IAE, e_{IAE} as defined in equation (30), was used to quantify the overall tracking accuracy of the system. The ORV system tracked the reference trajectory shown in figure 7(a) with an $e_{IAE} = 0.0209$ rad s.

$$e_{IAE} = \int |\theta_{ref} - \theta| \,. \tag{30}$$

Results from the simulation shown in figure 7(a) highlight accurate tracking until recruitment of the second FAM. This accuracy can be attributed to the ideal model assumption in both the feed forward controller and the plant. However, during the recruitment of the second muscle we can see that the arm experiences a significant 'dip' of 2 degrees.

There are two important physical phenomena that occur during the phase corresponding to this dip. The first of these phenomena is the 'dwell' state of FAM 2 where it does not get pressurized even though it is recruited as shown in figure 8(a).

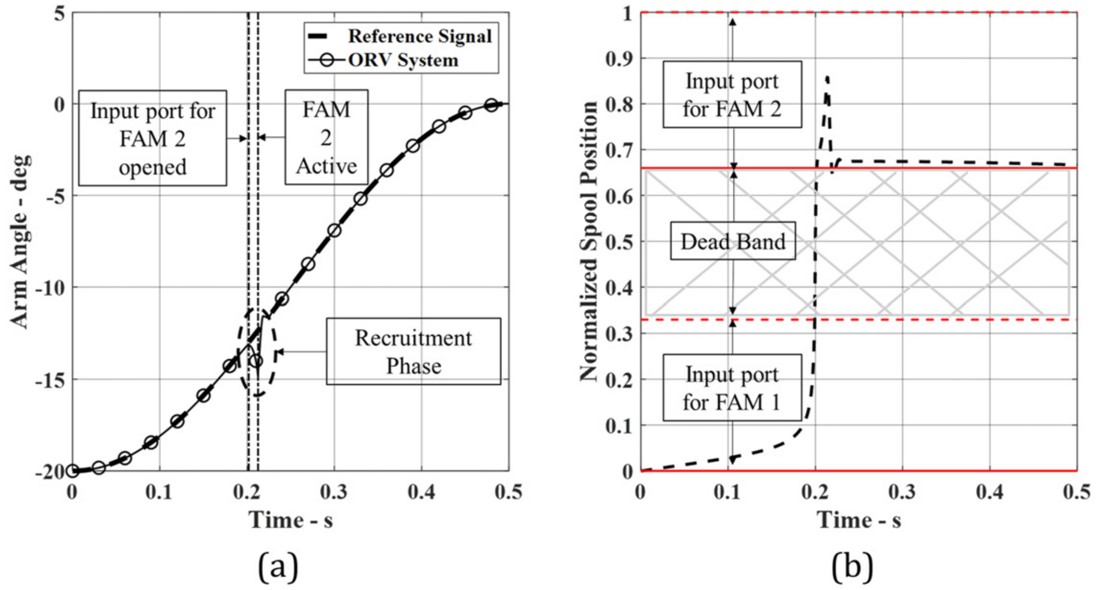

Figure 7. Simulation results for a trajectory of 0.5 s time period with $\Delta\theta = 20$ degrees (a) shows a comparison of the system arm angle rotation with the reference trajectory. (b) Shows the normalized position of the trailing end of the spool during the simulation.

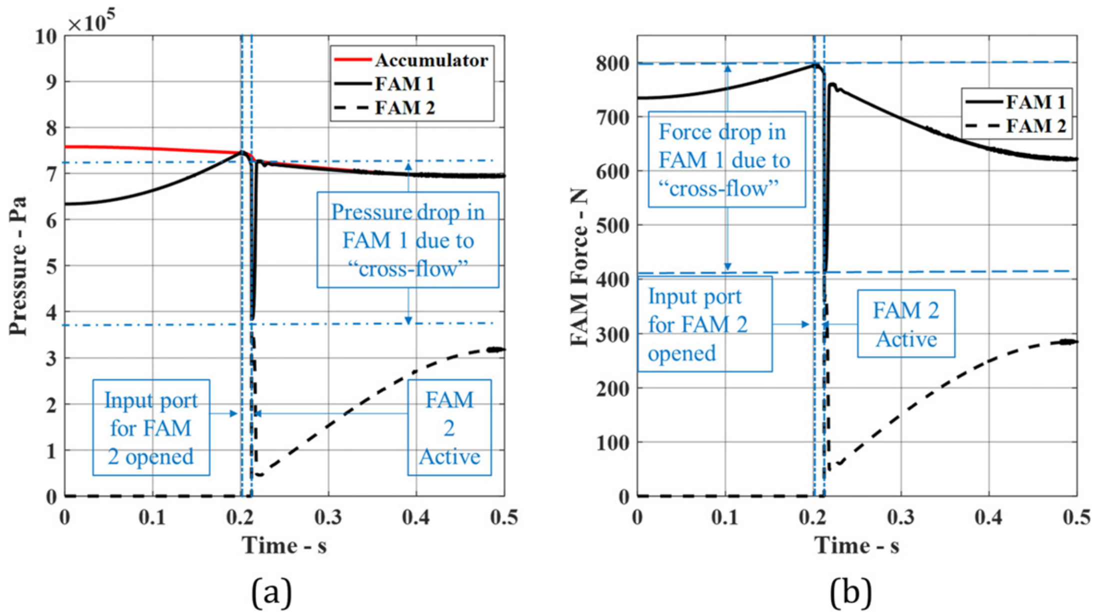

Figure 8. Simulation results for a trajectory of 0.5 s time period with $\Delta\theta = 20$ degrees (a) shows the pressure dynamics in FAM 1 and FAM 2 during the simulation, highlighting their important characteristics during the recruitment phase. (b) Shows the FAM forces and the drop in FAM 1 force during the recruitment phase.

Figure 9 shows that at the beginning of dwell state, FAM 2 is 'slack' since it has zero contraction and FAM 1 is at a contraction level corresponding to the arm angle, θ. This leads to a free-strain contraction rate x_{free} (equation (31)) of FAM 2 until it 'de-slacks' to the contraction level of FAM 1. During this de-slacking, FAM 2 does not exert any force as seen in figure 8(b).

$$\dot{x}_{\text{free}} = \frac{c_v x_{v,2}\sqrt{P_s - P_2} + Q_{f,12}}{\pi r_0^2 \left[a\left(1 - \frac{x_{\text{free}}}{l_0}\right)^2 - b\right]}. \tag{31}$$

Here $x_{v,2}$ is the port opening for input port of FAM 2, P_s is the supply pressure, P_2 is the pressure in FAM 2 and $Q_{f,12}$ is the cross flow between the FAM units as given in equation (4).

The other important phenomenon that occurs during the recruitment phase is the drop in the pressure of FAM 1 which corresponds to a drop in muscle force as shown in figure 6(b). This is due to the cross-flow $Q_{f,12}$ between the FAM ports during FAM 2 recruitment. It can be seen in figure 7(b) that the spool position is at the closing point of FAM 2's input

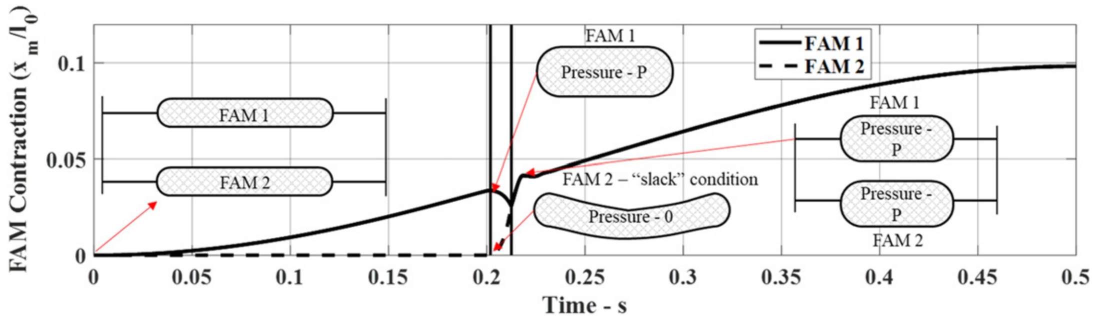

Figure 9. Different states of the FAM 1 and FAM 2 during the simulation highlighting the slack state FAM 2 during the recruitment phase.

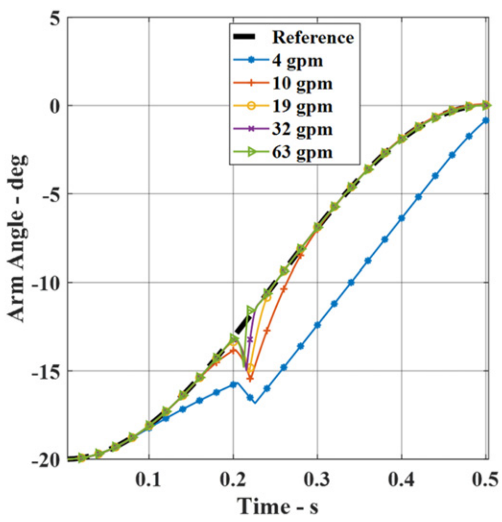

Figure 10. Simulation results for a trajectory of 0.5 s time period with $\Delta\theta = 20$ degrees based on different valves in the MOOG G761 series of valves with various nominal flow rates.

port which results in complete opening of FAM 1's input port. Since this occurs during the dwell phase of FAM 2, it creates a pressure differential across the FAM units which results in fluid flow from FAM 1 to FAM 2 resulting in a pressure drop in FAM 1.

The primary valve parameter that affects the dwell period of the recruitment phase is the nominal flow rate, Q_N of the valve. A series of simulations with valve parameters based on MOOG G761 series valves with varying Q_N between 4 lpm to 63 lpm, have been simulated to illustrate this effect. As seen in figure 10 with increasing Q_N the dwell region decreases. The valve with the lowest Q_N of 4 lpm is not able to track the reference trajectory as the required flow rate is greater than the maximum flow rate possible with the valve. Conversely, the valve with the highest Q_N of 63 lpm has the smallest dwell region.

3.4.2. Comparison of ORV and MVS

Existing research for AVR in hydraulic artificial muscles uses multiple valves to control a FAM bundle. The ability of an MVS to control the FAM units independently makes the MVS ideal in terms of performance. The cross-flow effect seen in ORV is absent in MVS as the FAM units are decoupled from each other.

An MVS with two independent and identical valves whose spool dynamics and sizing are equivalent to the ORV described in section 2.1.1 is shown in figure 11.

To compare both the valve systems, they are coupled with identical rotating arm FAM systems. In addition to identical plant models, equivalent controllers are also required to isolate the effects of the valve systems. Since an MVS has two valves, there are two controllers in the control system. The feed forward controller developed in section 3.2.2.1 for a single FAM unit remains relevant for the MVS since the individual system dynamics are identical in both the ORV and MVS. Hence, two identical feed forward controllers are implemented for both the valves in the MVS as shown in figure 12 with a supply pressure-based switching logic identical to the one presented in section 3.2.1 equation (20).

Figure 13 shows a trajectory tracking comparison between the ORV and MVS controlled system which reveals that the ORV performs better compared to the MVS in terms of the IAE ($e_{\mathrm{IAE,ORV}} = 0.0209$ rad s, $e_{\mathrm{IAE,MVS}} = 0.0737$ rad s). The primary driver for these results is the dwell region in the recruitment phase. The dwell region of MVS is longer compared to that of the ORV. This is because of the cross-flow in the ORV which leads to a faster pressurization of FAM 2 and therefore faster de-slacking of newly recruited FAM 2. The free strain contraction in the MVS is only due to the supply pressure whereas in the ORV both the supply and FAM 1 contribute.

Furthermore, a series of trajectories with an arm angle rotation varying between 45 degrees and 20 degrees varying in tip masses, m ranging from 1 kg to 2.2 kg over a time period of 0.5 s are simulated for both the valve systems. The ORV and MVS had an overall error of $e_{\mathrm{IAE,ORV}} = 0.1657$ rad s and $e_{\mathrm{IAE,MVS}} = 0.2213$ rad s respectively, averaged across the simulated conditions. These results show that the ORV is

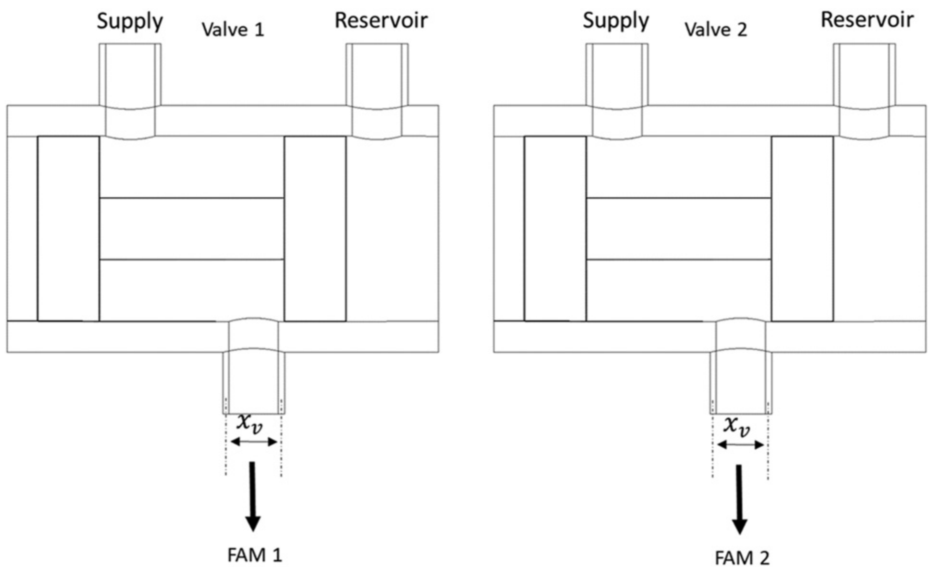

Figure 11. Schematic of the independent valve configuration of the MVS.

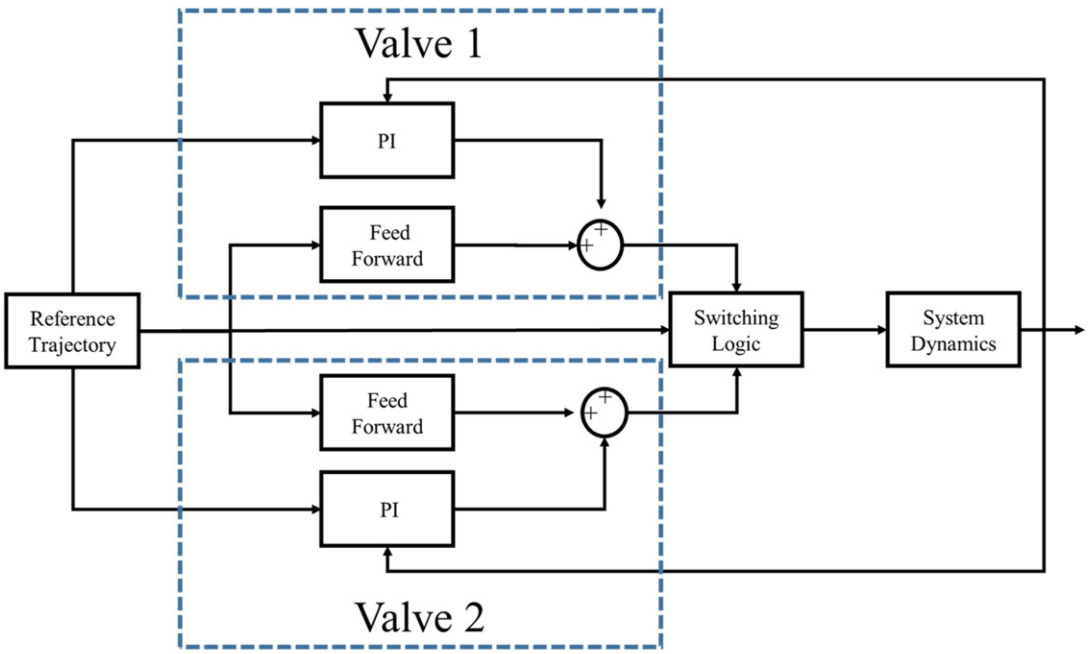

Figure 12. A simplified block diagram of the control system used to implement a model based feed forward PI controller in the MVS.

marginally better compared to MVS with respect to the IAE metric across a range of conditions.

3.4.3. Effects of switching logic tuning

The current switching logic determines that the recruitment of FAM 2 happens when FAM 1 reaches its maximum capacity i.e. when the required pressure is equal to the supply pressure. Until then, FAM 2 remains slack and at atmospheric pressure as the FAM 1 contracts. As seen in the previous results, this slack introduces a dwell region in the recruitment phase leading to degradation in trajectory tracking performance.

As possible means to address this, a modified switching logic with a threshold factor, k_{th}, ranging from 0 to 1 is introduced. With the threshold factor, the recruitment of FAM 2 is preceded by a priming state during which sufficient fluid is pumped into FAM 2 that will allow it to de-slack without getting pressurized thus keeping it passive. This phase begins when the required pressure reaches $k_{\mathrm{th}}P_{\mathrm{s}}$ as shown in equation (32). The lower the k_{th}, the earlier the priming state for FAM 2 happens thus contracting it ahead of when it is required. Table 2 shows the behavior of the FAMs during different recruitment states: state 1, 'priming', and state 2 (when the modified switching

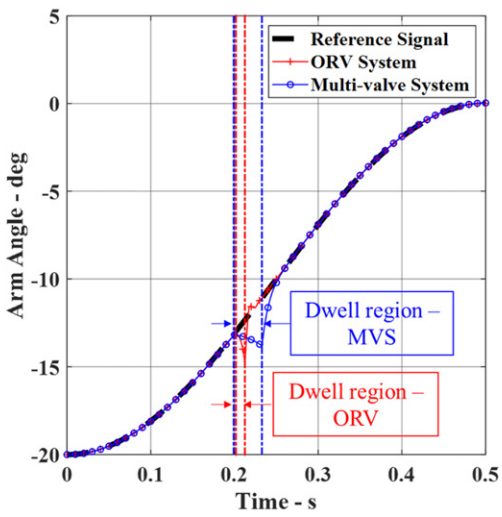

Figure 13. Simulation results show the comparison of trajectory tracking between ORV and MVS for a trajectory of 0.5 s time period with $\Delta\theta = 20$ degrees and $m = 2.2$ kg.

Table 2. Different states of recruitment with switching logic tuning.

		Recruitment State		
		1	Priming	2
Flow into	FAM 1	Yes	Yes	Yes
	FAM 2	No	Yes	Yes
Contraction of	FAM 1	Yes	Yes	Yes
	FAM 2	No	Yes	Yes
Force applied by	FAM 1	Yes	Yes	Yes
	FAM 2	No	No	Yes
Pressurized	FAM 1	Yes	Yes	Yes
	FAM 2	No	No	Yes

logic is implemented). It is important to note that the initial switching logic had only recruitment states 1 and 2.

$$\mathrm{RS} = \begin{Bmatrix} 1, P_{\mathrm{req}} < k_{\mathrm{th}} P_{\mathrm{s}} \\ 2, P_{\mathrm{req}} \geqslant k_{\mathrm{th}} P_{\mathrm{s}} \end{Bmatrix}. \tag{32}$$

The threshold factor study reveals trajectory tracking performance gains for the MVS and losses for ORV as shown in figure 14 and table 3. Due to the design of the ORV, the input port for FAM 1 opens to supply completely when priming FAM 2 thus rapidly increasing the pressure in FAM 1. Although the threshold factor enables earlier recruitment of FAM 2 by priming it ahead of its recruitment point, the gains due to this advancement are negated by the overshoot caused by the accelerated pressure growth in FAM 1 (figure 14(b)). There is a flexibility in control law for MVS since the FAM 1 can still be controlled independent of FAM 2. This allows for the valve of FAM 1 to maintain required pressure when FAM 2 is being primed. For the given trajectory, MVS has the best trajectory tracking performance for a k_{th} of 0.8 (80% threshold factor).

These results show that the lower the threshold factor the better the trajectory tracking performance. This is found out to be true across a range of operating conditions, $\Delta\theta = 20$–45 degrees and $m = 1$–2.2 kg, when simulated with lower threshold factors as shown table 4, which shows the average IAE of all the operating conditions.

As seen earlier at $k_{\mathrm{th}} = 1$ the average trajectory tracking errors of ORV and MVS are $e_{\mathrm{IAE,ORV}} = 0.1657$ rad s and $e_{\mathrm{IAE,MVS}} = 0.2213$ rad s respectively. However, by tuning the switching logic the average trajectory tracking error for MVS, $e_{\mathrm{IAE,MVS}}$, is minimized to 0.1346 rad s at $k_{\mathrm{th}} = 0.4$.

3.4.4. System efficiency with different valve configurations

In addition to tracking accuracy, hydraulic system efficiency is also an important parameter to evaluate the implications of the valve architecture. Efficiency of the hydraulic system, η is defined as the ratio of mechanical work output and fluid energy input to the FAM bundle. The output of the bundle is mechanical work done by the FAMs, W_{bundle} and fluid energy input to the valve and actuation system, E_{in}.

Energy consumption due to fluid compression was considered to be negligible since the operating fluid is assumed to have a high bulk modulus. This definition of efficiency dictates that the system is the most efficient when the FAMs operate near the supply pressure and its efficiency degrades when the FAMs are operating at lower pressures. The work done by the actuators in rotating the arm is the total work done by the FAM actuators as shown in equation (33).

$$W_{\mathrm{bundle}} = \int F_{m,1}\dot{x}_{m,1}\,\mathrm{d}t + \int F_{m,2}\dot{x}_{m,2}\,\mathrm{d}t, \tag{33}$$

$$E_{\mathrm{in}} = \int P_{\mathrm{s}}(\dot{V}_{m,1} + \dot{V}_{m,2})\,\mathrm{d}t. \tag{34}$$

The fluid energy input is the work done by the accumulator to drive the volume change in the FAMs as given in equation (34). Simulations across a range of operating conditions show comparable efficiencies using both the valve systems as seen in figure 15. Overall efficiencies for ORV and MVS are 0.5242 and 0.4922 respectively when averaged over a range of operating conditions with a 0.5 s time period trajectories of $\Delta\theta = 20$–45 degrees and $m = 1$–2.2 kg. It is important to note that these simulations are done without tuning the switching logic for MVS, i.e. $k_{\mathrm{th}} = 1$.

To identify trade-offs between efficiency and trajectory tracking performance using a non-unity threshold factor for MVS, the same set of operation conditions were simulated with different threshold factors. Average efficiencies decrease with lower threshold factors, as shown in figure 16. This is further illustrated in table 5, which shows the average efficiencies of all the operating conditions with different threshold factors.

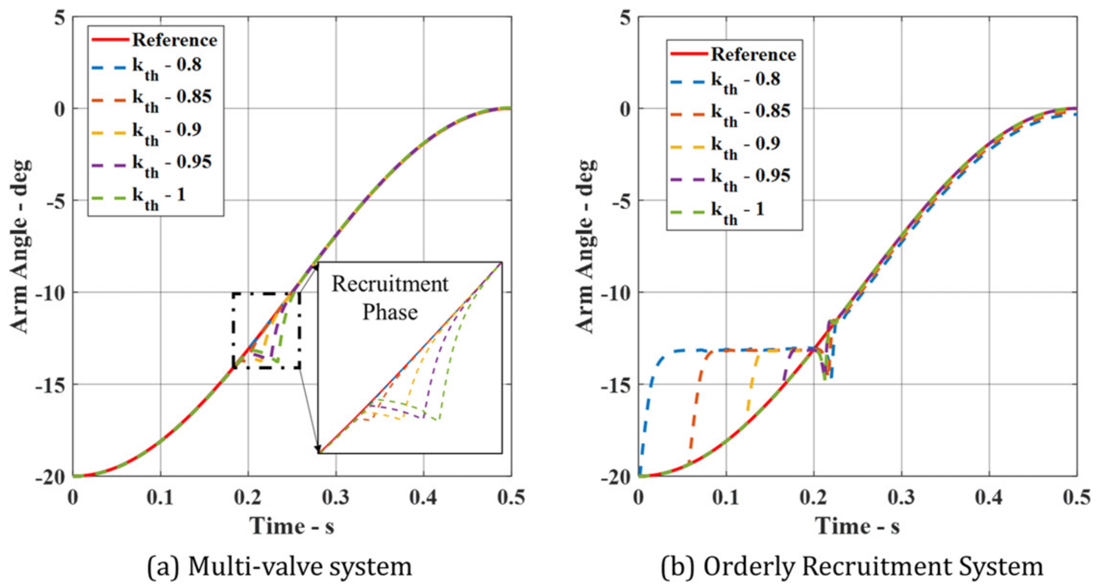

Figure 14. Simulation results for trajectories of 0.5 s time period with $\Delta\theta = 20$ degrees, $m = 2.2$ kg and a range of threshold factors (a) shows improvement in the tracking performance of MVS with lower threshold factors and (b) shows deterioration in the tracking performance of ORV with lower threshold factors.

Table 3. Trajectory tracking error for 0.5 s trajectory $\Delta\theta = 20$ degrees, $m = 2.2$ kg.

Threshold factor-k_{th}	100%	95%	90%	85%	80%
IAE–MVS	0.0737	0.0547	0.0345	0.0124	0.0057
IAE–ORV	0.0209	0.0443	0.1655	0.5208	0.9281

Table 4. Average trajectory tracking error for MVS, $\Delta\theta = 20$–45 degrees, $m = 1$–2.2 kg.

Threshold factor-k_{th}	100%	80%	60%	40%
Average IAE	0.2213	0.2174	0.1658	0.1346

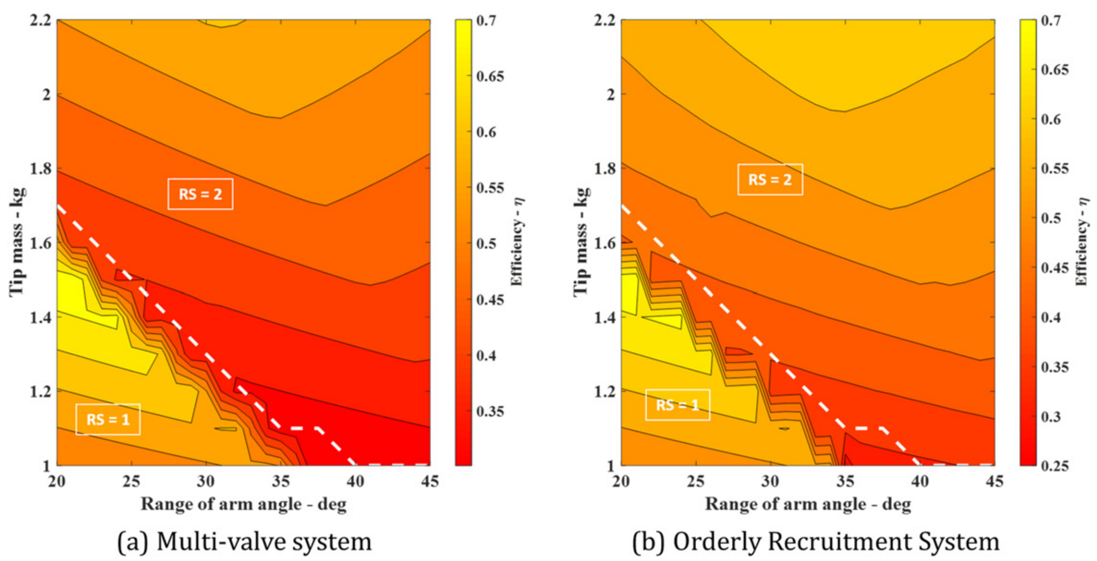

Figure 15. Simulation results for efficiencies of (a) MVS and (b) ORV system across a range of $\Delta\theta = 20$–45 degrees, $m = 1$–2.2 kg and $k_{th} = 1$.

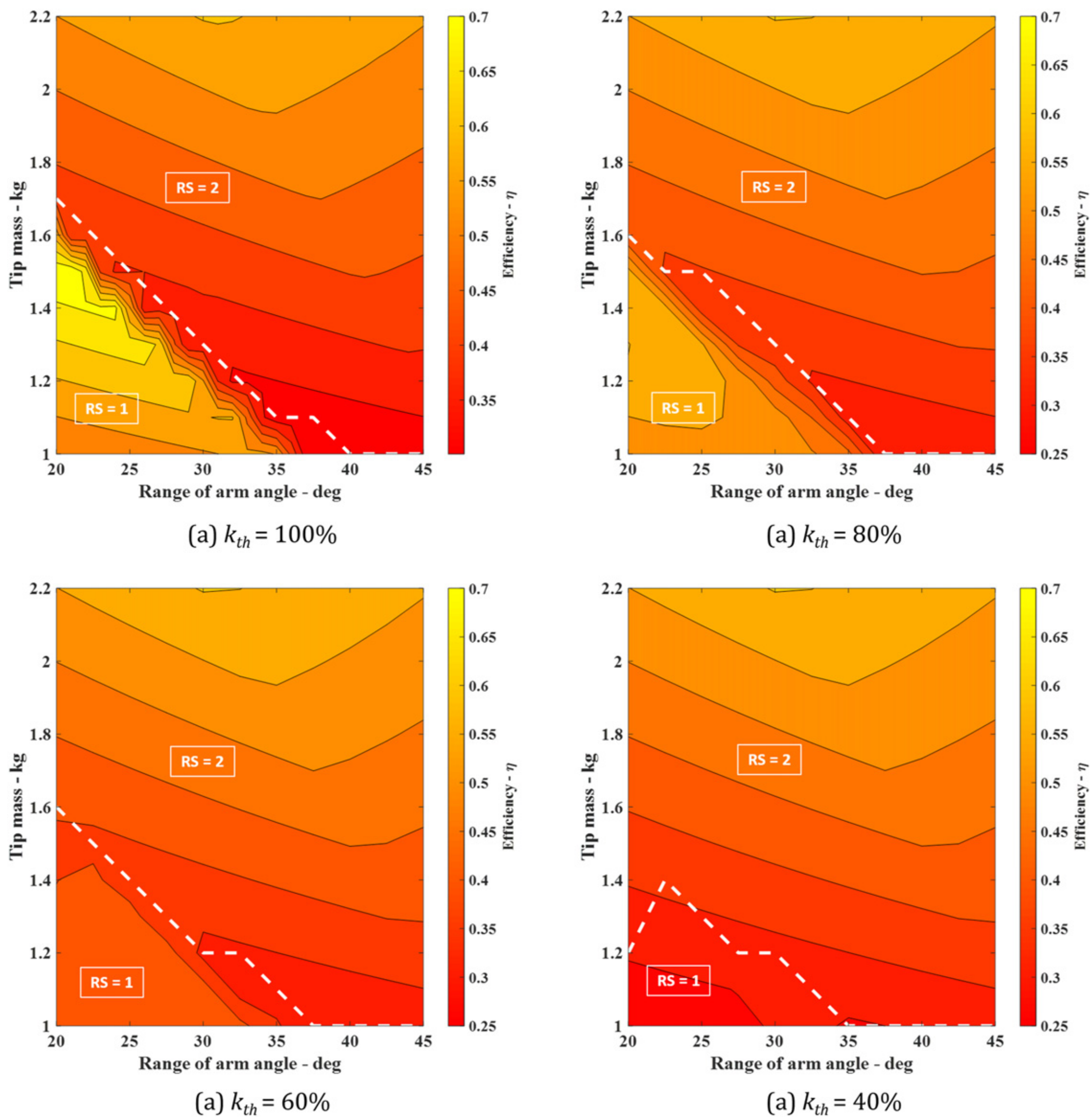

Figure 16. Simulation results for efficiencies of MVS across a range of $\Delta\theta = 20$–45 degrees and $m = 1$–2.2 kg with threshold factors of (a) 100% (b) 80% (c) 60% (d) 40%.

Table 5. Average hydraulic system efficiency for MVS with different threshold factors and a range operating conditions—$\Delta\theta = 20$–45 degrees and $m = 1$–2.2 kg.

Threshold factor-k_{th}	100%	80%	60%	40%
Average efficiency-η	0.4922	0.4790	0.4567	0.4411

These results highlight the trade-offs between trajectory tracking performance and hydraulic efficiencies of the MVS. As seen in section 3.4.1, the ORV system had an average IAE, $e_{\mathrm{IAE,ORV}} = 0.1657$ rad s^{-1}. For a comparable trajectory tracking performance from the MVS a threshold factor of 0.6 was required (average $e_{\mathrm{IAE,MVS}} = 0.1658$ with $k_{\mathrm{th}} = 0.6$). However, at $k_{\mathrm{th}} = 0.6$ hydraulic efficiency of MVS is 0.4567 which is nearly 13% when compared with an ORV system, which has 0.5242 efficiency.

4. Conclusions

The primary focus of this research is to design and develop a novel ORV that implements bio-inspired sequential motor unit recruitment in a single-valve system. The paper first presents a detailed analytical model of the ORV and its unique design characteristics. The dynamics of an ORV-controlled FAM bundle are simulated and validated through a proof-of-concept experiment to show the ORV's ability to sequentially activate FAMs within a variable recruitment bundle as well as its cross-flow effect. To further explore the functionality of an ORV, a case study of an electrohydraulic system in conjunction with a 1-DOF robot arm is simulated. Analytical models for all the subsystems in the plant model were developed with sufficient fidelity to capture the different dynamics of the system.

The orderly recruitment strategy was embedded into a model-based feed forward controller. This controller was designed to anticipate the required input while fully considering the dynamics of the system. Furthermore, the performance of the ORV system with its feed forward controller was demonstrated through a series of trajectory tracking simulations. These simulations revealed some loss in tracking accuracy during the recruitment phase of the system with a significant dip in the trajectory. The recruitment phase of the system revealed the unique flow and spool dynamics of the ORV. To further benchmark the performance of the ORV it was compared to a conventional MVS with equivalent dynamics and controller. Initial comparisons showed that the ORV, due to its distinctive characteristics like the cross-flow, had a lower overall tracking error compared to the MVS.

Tuning of the recruitment state switching logic was explored as a potential way to improve the tracking accuracy of the system. For the MVS, significant improvement in the tracking performance was obtained by using a threshold factor to trigger priming of the second FAM ahead of its recruitment. This approach is readily implemented in the MVS due its multiple independent valves, but not practical in the ORV system. Furthermore, this priming approach was found to decrease system efficiency. Specifically, when tuned for equivalent tracking performance, the MVS system with threshold factor was approximately 13% less efficiency than the ORV system.

To conclude, the paper presents a novel ORV concept which can be used to implement an AVR strategy with a simpler setup while preserving a balance of trajectory tracking performance and hydraulic system efficiency.

Funding

This work was supported primarily by the Faculty Early Career Development Program (CAREER) of the National Science Foundation under NSF Award No. 1845203 and Program Manager Irina Dolinskaya. Additionally, this material is based upon work supported by the National Science Foundation Graduate Research Fellowship Program under Grant No. 1650114. Any Opinions, findings and conclusions or recommendations expressed in this material are those of the author(s) and do not necessarily reflect those of the National Science Foundation.

Data availability statement

The data that support the findings of this study are available upon reasonable request from the authors.

ORCID iDs

Dheeraj Vemula https://orcid.org/0000-0002-5834-5541
Jeong Yong Kim https://orcid.org/0000-0001-9895-9807
Nicholas Mazzoleni https://orcid.org/0000-0002-9377-849X

References

[1] Tondu B 2012 Modelling of the McKibben artificial muscle: a review *J. Intell. Mater. Syst. Struct.* **23** 225–53
[2] Ramsey R W and Street S F 1940 The isometric length-tension diagram of isolated skeletal muscle fibers of the frog *J. Cell. Comp. Physiol.* **15** 11–34
[3] Mori M, Suzumori K, Takahashi M and Hosoya T 2010 Very high force hydraulic McKibben artificial muscle with a p-phenylene-2,6-benzobisoxazole cord sleeve *Adv. Robot.* **24** 233–54
[4] Zhang Z and Philen M 2012 Pressurized artificial muscles *J. Intell. Mater. Syst. Struct.* **23** 255–68
[5] Tiwari R, Meller M A, Wajcs K B, Moses C, Reveles I and Garcia E 2012 Hydraulic artificial muscles *J. Intell. Mater. Syst. Struct.* **23** 301–12
[6] Tondu B, Ippolito S, Guiochet J and Daidie A 2005 A seven-degrees-of-freedom robot-arm driven by pneumatic artificial muscles for humanoid robots *Int. J. Robot. Res.* **24** 257–74
[7] Andrikopoulos G, Nikolakopoulos G and Manesis S 2011 A survey on applications of pneumatic artificial muscles *2011 19th Mediterranean Conf. Control & Automation (MED)* (IEEE) pp 1439–46
[8] Chang M-K 2010 An adaptive self-organizing fuzzy sliding mode controller for a 2-DOF rehabilitation robot actuated by pneumatic muscle actuators *Control Eng. Pract.* **18** 13–22
[9] Jiang X, Xiong C, Sun R, Huang X and Xiong Y 2011 Static and dynamic characteristics of rehabilitation joint powered by pneumatic muscles *Ind. Robot: Int. J.* **38** 486–91
[10] Robinson R M, Kothera C S and Wereley N M 2014 Variable recruitment testing of pneumatic artificial muscles for robotic manipulators *IEEE/ASME Trans. Mechatronics* **20** 1642–52
[11] Wu J, Huang J, Wang Y and Xing K 2013 Nonlinear disturbance observer-based dynamic surface control for trajectory tracking of pneumatic muscle system *IEEE Trans. Control Syst. Technol.* **22** 440–55
[12] Meller M A, Bryant M and Garcia E 2014 Reconsidering the McKibben muscle: energetics, operating fluid, and bladder material *J. Intell. Mater. Syst. Struct.* **25** 2276–93
[13] Buchthal F and Schmalbruch H 1980 Motor unit of mammalian muscle *Physiol. Rev.* **60** 90–142
[14] Henneman E, Somjen G and Carpenter D O 1965 Excitability and inhibitibility of motoneurons of different sizes *J. Neurophysiol.* **28** 599–620
[15] Bryant M, Meller M A and Garcia E 2014 Variable recruitment fluidic artificial muscles: modeling and experiments *Smart Mater. Struct.* **23** 074009
[16] Meller M, Chipka J, Volkov A, Bryant M and Garcia E 2016 Improving actuation efficiency through variable recruitment hydraulic McKibben muscles: modeling, orderly recruitment control, and experiments *Bioinspir. Biomim.* **11** 065004
[17] Chapman E M, Jenkins T and Bryant M 2018 Design and analysis of electrohydraulic pressure systems for variable recruitment in fluidic artificial muscles *Smart Mater. Struct.* **27** 105024

[18] Manring N D and Fales R C 2019 *Hydraulic Control Systems* (New York: Wiley)

[19] Jelali M and Kroll A 2012 *Hydraulic Servo-Systems: Modelling, Identification and Control* (Berlin: Springer)

[20] Tondu B and Lopez P 2000 Modeling and control of McKibben artificial muscle robot actuators *IEEE Control Syst. Mag.* **20** 15–38

[21] Klute G K and Hannaford B 2000 Accounting for elastic energy storage in McKibben artificial muscle actuators *J. Dyn. Syst. Meas. Control* **122** 386–8

[22] Kothera C S, Jangid M, Sirohi J and Wereley N M 2009 Experimental characterization and static modeling of McKibben actuators *J. Mech. Des.* **131** 091010

[23] Ball E and Garcia E 2016 Effects of bladder geometry in pneumatic artificial muscles *J. Med. Devices* **10** 041001

[24] Yu Z, Pillsbury T, Wang G and Wereley N M 2019 Hyperelastic analysis of pneumatic artificial muscle with filament-wound sleeve and coated outer layer *Smart Mater. Struct.* **28** 105019

[25] Kim J Y, Mazzoleni N and Bryant M 2021 Modeling of resistive forces and buckling behavior in variable recruitment fluidic artificial muscle bundles *Actuators* **10** 42 (Multidisciplinary Digital Publishing Institute)

[26] De Volder M, Moers A J M and Reynaerts D 2011 Fabrication and control of miniature McKibben actuators *Sensors Actuators* A **166** 111–6

[27] Xiang C, Giannaccini M E, Theodoridis T, Hao L, Nefti-Meziani S and Davis S 2016 Variable stiffness Mckibben muscles with hydraulic and pneumatic operating modes *Adv. Robot.* **30** 889–99

[28] Meller M, Kogan B, Bryant M and Garcia E 2018 Model-based feedforward and cascade control of hydraulic McKibben muscles *Sensors Actuators* A **275** 88–98

[29] Gholizadeh H, Burton R and Schoenau G 2011 Fluid bulk modulus: a literature survey *Int. J. Fluid Power* **12** 5–15